Efficiency of Hole Transfer from Photoexcited Quantum Dots to Covalently Linked Molecular Species

Tina X. Ding[†⊥§], **Jacob H. Olshansky**[†⊥§], **Stephen R. Leone**[†‡∥], **and A. Paul Alivisatos***[†⊥§]

[†]Department of Chemistry, [‡]Department of Physics, University of California, Berkeley, Berkeley, California 94720, United States

[⊥]Material Sciences Division and [∥]Chemical Sciences Division, Lawrence Berkeley National Laboratory, Berkeley, California 94720, United States

[§]Kavli Energy Nanosciences Institute, Berkeley, California 94720, United States

J. Am. Chem. Soc., **2015**, *137* (5), pp 2021–2029

DOI: 10.1021/ja512278a

Publication Date (Web): January 15, 2015

apalivisatos@lbl.gov

•

Abstract

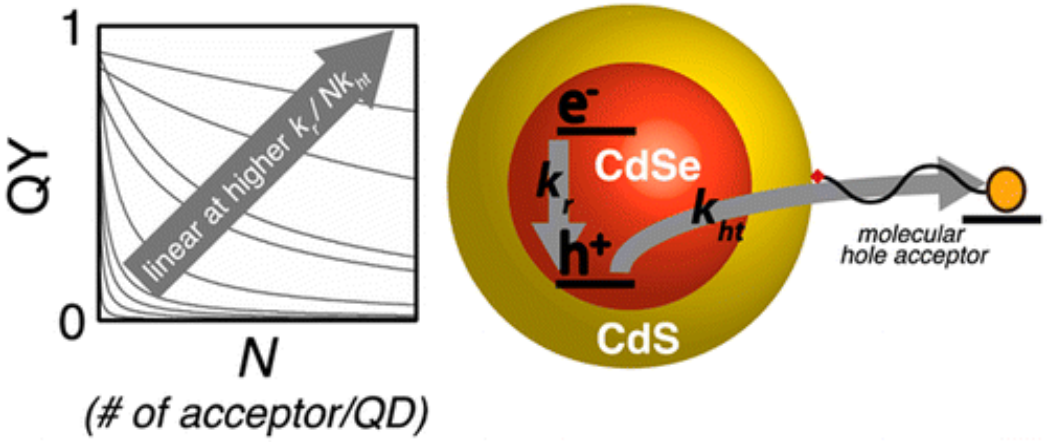

Hole transfer from high photoluminescence quantum yield (PLQY) CdSe-core CdS-shell semiconductor nanocrystal quantum dots (QDs) to covalently linked molecular hole acceptors is investigated. ^{1}H NMR is used to independently calibrate the average number of hole acceptor molecules per QD, *N*, allowing us to measure PLQY as a function of *N*, and to extract the hole transfer rate constant per acceptor, k_{ht}. This value allows for reliable comparisons between nine different donor–acceptor systems with variant shell thicknesses and acceptor ligands, with k_{ht} spanning over 4 orders of magnitude, from *single* acceptor time constants as fast as 16 ns to as slow as 0.13 ms. The PLQY variation with acceptor coverage for all k_{ht} follows a universal equation, and the

shape of this curve depends critically on the ratio of the total hole transfer rate to the sum of the native recombination rates in the QD. The dependence of k_{ht} on the CdS thickness and the chain length of the acceptor is investigated, with damping coefficients β measured to be (0.24 ± 0.025) $Å^{-1}$ and (0.85 ± 0.1) $Å^{-1}$ for CdS and the alkyl chain, respectively. We observe that QDs with high intrinsic PLQYs (>79%) can donate holes to surface-bound molecular acceptors with efficiencies up to 99% and *total* hole transfer time constants as fast as 170 ps. We demonstrate the merits of a system where ill-defined nonradiative channels are suppressed and well-defined nonradiative channels are engineered and quantified. These results show the potential of QD systems to drive desirable oxidative chemistry without undergoing oxidative photodegradation.

•

Introduction

By leveraging the development of foundational nanoscience concepts of quantum confinement in semiconductor nanocrystals, today we have a generation of colloidal quantum dots (QDs) that are robust and bright light emitters. These colloidal QDs have important applications as optically excited biological luminescent probes(1) and as highly energy efficient down-converters for green and red emission in displays.(2) In recent years, there has been widespread interest in using QDs in applications beyond light emission, as light absorbers for solar energy applications where the photoexcited charges in the QD are transferred to other species as a form of energy conversion and storage.(3, 4) When it comes to this nanocrystal charge transfer process, there still exist many unresolved issues at a fundamental level. While the development of Marcus electron transfer theory has clarified the field of molecular charge transfer,(5, 6) the same level of understanding and agreement has not yet been achieved for its nanocrystal analogue.(7) A growing body of spectroscopic work has examined charge transfer rates from QDs to molecular charge acceptors typically physisorbed onto the QD surface, exploring the parameter space in the Marcus equation.(8) Electron transfer studies(8-13) outnumber hole studies,(14-19) despite hole transfer being the limiting factor in the efficiencies of QD sensitized solar cells and in QD-based colloidal photocatalytic hydrogen evolving systems.(20, 21)

To establish a sound model for charge transfer from nanocrystals to molecular acceptors, we must address the features of this system that make the process more difficult to characterize than that of the pure molecular case. In addition to the intrinsic intensive parameters of the Marcus model, such as the driving force, the electronic coupling between donor and acceptor, and inner-sphere and outer-sphere reorganization energies, in QDs one must also contend with the possible presence of trap states of unknown energetic and spatial distribution on the QD surface,(22, 23) and with the need to precisely quantify the number of molecular acceptors attached to the QD.

The presence of ill-defined trap states can be ameliorated by growing a shell of a

larger bandgap material around the QD. Although the nonradiative pathways are now more suppressed, the shell also electronically insulates the QD, erecting a barrier to the very charge transfer process for which it is designed. The careful balance of these two interplaying processes of mitigating undesirable traps while enhancing desirable traps is key to the photoenergy conversion applications of these QD systems.

In addition, the second unique characteristic of QD charge transfer is that a single QD can attach to one to tens of thousands of molecular acceptors, depending on the QD size and native ligands. In measuring this extensive parameter N, the average number of bound charge acceptors per QD, the single donor-single acceptor charge transfer rate k_{ht}, is deconvoluted from the ensemble charge transfer rate Nk_{ht} (eq 1). In eq 1, we assume that each additional hole transfer pathway is additive and independent of the other pathways of the system. At high coverage, we expect that there may be positive or negative cooperativity leading to deviations from this assumption.

$$k_{Nht} = Nk_{ht} \quad (1)$$

We note that, without knowledge of k_{ht}, comparisons between systems with varying driving force and coupling are difficult, as the surface energetics and ligand binding equilibria vary as the nanocrystals change size, shape, and composition.(24-26) Literature values compiled by Knowles et al. for electron transfer rates vary from femtoseconds to nanoseconds while hole transfer rates are typically slower, but with just as large a dynamic range.(8) As noted in the review, inconsistencies in the method of measurement, especially regarding reporting single donor-single acceptor charge transfer rate constants (k_{ht}) versus single donor-multiple acceptor charge transfer rate constants (k_{Nht}), lead to drastically different values for similar systems. Some groups have characterized the number of ligands bound indirectly using optical methods.(10, 16, 26-28) In most of these previous studies, fitting based on a binding model that differentiates bound and free states is used to indirectly infer N. NMR, though difficult to measure due to the high concentration required for its measurement, allows one to directly differentiate between bound versus free ligands due to their different signatures in the NMR spectrum.

In this paper, we examine the transfer of photoexcited holes from quasi-type-II symmetric (nearly spherical) CdSe-core CdS-shell to a quantified number of molecular acceptors on the QD surface, to clarify the limitations and efficiencies of such a system. We measure the photoluminescence quantum yield (PLQY) as a function of N, from which we extract k_{ht} for nine donor–acceptor systems, with k_{ht} spanning over 4 orders of magnitude to demonstrate the highly variant effect of N on the PLQY for these systems.

In doing so, we clarify a topic of great inconsistency in the literature regarding the PLQY–N relationship. Frequently, PL intensity has been used as a direct (linear) proxy for coverage or surface binding,(29-31) yet there have also been reports

that the dependence is nonlinear(32, 33) with coverage. We show that different limits of the ratio of Nk_{ht} to the sum of the rate constants for the intrinsic pathways account for the conflicting linear to nonlinear literature findings.
In these systems, k_{ht} exhibit characteristic lifetimes from tens of nanoseconds to hundreds of microseconds. The former is highly competitive with the radiative lifetime of the nanocrystal while the latter is completely ineffective at extracting charge on a one-acceptor basis but effective at high N limits. In these experiments, we address the unique characteristics of nanocrystal charge transfer that have been discussed in the preceding paragraphs, to show that these subtle parameters can have significant effects on the efficiency for hole transfer, an important consideration in photochemical energy conversion.
•

Results and Discussion

Description of Donor–Acceptor System

CdSe samples (3.9 nm diameter) with 3 monolayer (ML; 1 ML = 0.35 nm), 5 ML, and 7 ML CdS shells (Figure 1c–f) were synthesized, and their absorbance and fluorescence spectra are plotted in Figure 1a. The PLQYs and radiative rate constants, k_r's, for these nanocrystals are 79%, 86%, 91%, and 0.044, 0.031, 0.021 ns^{-1}, respectively. The decreasing values of k_r as a function of increasing particle size are expected as a result of the electron delocalization through the larger volumes, resulting in reduced wave function overlap with the hole that remains localized in the CdSe core.(34)

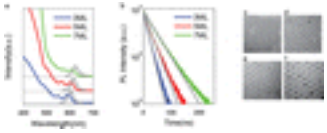

Figure 1. Optical and morphological characterization of CdSe-core CdS-shell nanocrystals. (a) Absorption and photoluminescence(gray) spectra of nanocrystals synthesized with the same 3.9 nm CdSe core with 3, 5, and 7 ML CdS shells. (b) Photoluminescence lifetime of the three core–shell particles with their respective single exponential fits (gray). (c–f) Transmission electron microscopy images of the CdSe core (c), and the three core–shell particles (d–f). Scale bar is 20 nm.

We examine hole transfer from the CdSe core to acceptors covalently linked to the nanocrystal surface via the thiolate binding group (Figure 2). The hole acceptor used is ferrocene, whose oxidation potential lies approximately 850 meV above the valence band of the CdSe core based on a previous measurement.(19) The large thermodynamic driving force for photoinduced hole transfer allows this process to compete with native radiative recombination. This is reflected in the measured PL(35) and PL lifetime,(19) yet the hole transfer rate in our study is most sensitive to modulations in the electronic coupling, achieved by varying the thickness and composition of the barrier material between the

CdSe core and the acceptor. We preclude the possibility of resonance energy transfer due to the lack of spectral overlap of the ferrocene absorption with QD emission. We also preclude electron transfer because the LUMO of ferrocene lies much higher than the conduction band of CdS and CdSe. (It is approximately 2.7 eV higher than the ferrocene HOMO position shown in Figure 2c.) Therefore, we attribute the dominant pathway for the quenching of the PL intensity and the decrease in the PL lifetime to hole transfer from CdSe to surface attached ferrocene. It is also assumed that the intrinsic nonradiative rates are negligibly affected by the presence of the added ligands. The donor–acceptor distance is well-defined in our system, achieved by using a nearly spherical nanocrystal morphology and acceptors that contain well-characterized binding groups. This expected well-defined distance is further verified in this study, as we use two ferrocene ligands with different alkyl chain lengths, 3-ferrocenylpropanethiol (FcC3SH) and 6-ferrocenylhexanethiol (FcC6SH), to demonstrate that the charge transfer rate constants match what would be expected for tunneling through saturated alkyl chains. We also examine the effects of the thiolate regarding hole transfer by using a thiol alkyl ligand with an NMR tag: 11-(1*H*-pyrrol-1-yl) undecane-1-thiol (PyrrSH). Although the pyrrole group has a 100 meV driving force for hole transfer (Supporting Information), the 11 carbon chain distance precludes pyrrole oxidation from being a significant hole transfer pathway, as the already low rate associated with the weak driving force is now diminished completely by an exponential dropoff in the rate across such a large distance. Therefore, PyrrSH is referred to as AlkylSH in the rest of this paper and functions as a control for examining hole transfer to surface thiols, a well-known shallow hole trap for CdSe materials.(36)

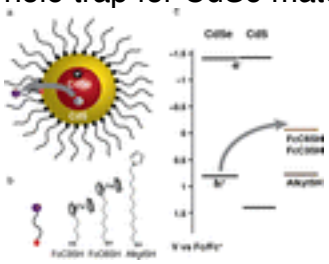

Figure 2. Donor–acceptor system. (a) The hole donor is at the CdSe core, and the acceptor is localized at the end of the ligand chain. (b) Hole acceptors FcC3SH, FcC6SH, and AlkylSH. (c) Energy positions of the conduction and valence bands of CdSe and CdS and the oxidation potentials of FcSH and AlkylSH.

The donor–acceptor system was prepared by controlled ligand exchange of FcC3SH, FcC6SH, or AlkylSH with the native oleate ligand. By varying the concentration of added functional thiols, QDs with a range of coverages were prepared and their PLQYs measured. Inductively coupled plasma (ICP) atomic emission spectroscopy combined with quantitative ^{1}H NMR(37) was used to determine the number of bound ligands per nanocrystal, *N*, whether it be native oleic acid, FcC3SH, FcC6SH, or AlkylSH. All ligands measured here have

spectrally resolved signatures in ^{1}H NMR that allow for facile quantification (Figure 3). ^{1}H NMR and ^{31}P NMR also revealed that the native nanocrystal surface contains bound oleate (the coordinating ligand in the Cd precursor) as well as octadecylphosphonate (ODPA, the CdSe core's surface ligand). ODPA has been shown to form very strong bonds on chalcogenide nanocrystal surfaces,(38, 39) and therefore, ODPA is a strong competitor for the surface of the final core–shell nanocrystal despite its overall lower concentration in the growth reaction. The presence of a consistent number of bound ODPA molecules (originating from the core ligands) in the synthesis of these core–shell nanocrystals with three shell thicknesses results in a deviation in the total number of bound oleic acids for the three sizes from what is predicted on the basis of their surface area. See Supporting Information for more detailed characterizations of the ligand environment before, during, and after ligand exchange (Supporting Information Table S1).

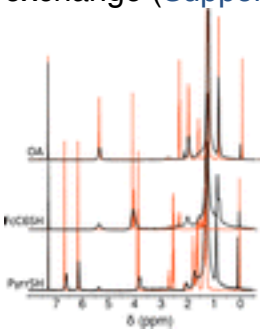

Figure 3. ^{1}H NMR spectra of the bound (black) and free (red) oleic acid (OA), FcC6SH, and PyrrSH. Distinctive peaks at 5.35 ppm (OA), 4.05 ppm (FcC6SH), and 6.15 ppm (AlkylSH) were used to quantify the number of ligands bound per nanocrystal. FcC3SH appears also at 4.05 ppm, but is broader due to it being closer in distance to the nanocrystal surface (Supporting Information).

We measured the QD PLQY as a function of N across nine donor–acceptor systems with k_{ht} spanning over 4 orders of magnitude (Figure 4). The nine k_{ht} values were controlled by electronic coupling. The effect of electronic coupling on charge transfer was modulated by varying the thickness of the CdS shell and the alkyl chain length of the ferrocene hole acceptor, both of which act as tunneling barriers for the holes that are energetically confined to the CdSe core. The nine systems represent all permutations possible from the three donor nanocrystals and three acceptor molecules used in this study, allowing us to compare the rates quantitatively across different coupling regimes.

$$\mathrm{PLQY_{AVG}} = \frac{k_r}{k_r + k_{nr} + Nk_{ht}} = \frac{k_r}{k_{tot}} \quad (2a)$$

$$\mathrm{PLQY_{POISSON}} = \sum_{n=0}^{N_{max}} \frac{N^n e^{-N}}{n!} \frac{k_r}{k_r + k_{nr} + nk_{ht}} \quad (2b)$$

The raw data (PLQY, N) of each of the nine systems is fit to eq 2a, which

describes the PLQY as a function of the rate constants of all the pathways of the photoseparated charges and N to yield the hole transfer rate constant per acceptor, k_{ht}, for that given system. The fit uses the radiative rate constant, k_r, and the nonradiative rate constant, k_{nr}, that have been determined for the native QD from PLQY and fluorescence lifetime measurements (Figure 1b). We also show that this is valid since k_r remains the same upon ligand exchange (Supporting Information Figure S3). The lifetime data fit well to single exponentials (Figure 1b) across the highest two decades of intensities, as expected from these core–shell materials,(40) and the fit is used to determine k_{tot}. Additionally, although the Poisson factor in eq 2b accurately describes the system, it has a negligible effect on the relationship for all systems except the two with the most efficient charge transfer with N less than 10 (Supporting Information Figure S4). For these reasons, eq 2a will be used for all further analysis. The raw data and their respective fits are plotted together in Figure 4. The same relationship plotted on a logarithmic scale for N is shown in the inset, allowing us to better visualize the expected quenching due to charge transfer for N being 1 to 10, which is significant for the systems containing FcC3SH as the acceptor. The fits in Figure 4 agree well with the data across the nine different systems even at high coverages, thereby confirming the validity of eq 1. For these systems, the presence of ODPA on the QD and the weaker packing efficiency of the ferrocene ligands relative to the native oleic acid molecules prevent the QD from achieving the intimate ligand interactions on the surface that may lead to cooperativity.

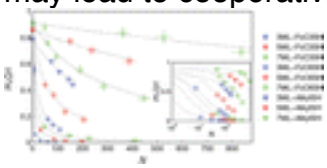

Figure 4. PLQY as a function of bound acceptor ligands per QD(N) for the nine donor–acceptor systems made with three donor particles and three acceptor molecules. Their rate constants are tabulated in Table 1. The fit to eq 2a is plotted in dashed black. Inset: the same data and fit is plotted on a logarithmic scale in the x axis to give a better representation of the effect of low N.

Table 1. Rate Constants, Surface Ligand Characterizations, and $HTQY_{max}$ of the Nine Donor–Acceptor Systems Plotted in Figure 4

	HT system	k_{ht} (ns^{-1})	OA$_o$	N_{max}	$N_{max}k_{ht}$ (ns^{-1})	k_r (ns^{-1})	$HTQY_{max}$
1a	3 ML-FcC3SH	0.063×10^{0}	198	91	5.8	0.044	99.0%
1b	5 ML-FcC3SH	0.010×10^{0}	413	197	2.0	0.031	98.2%
1	7 ML-FcC3SH	0.026×10^{-1}	89	411	1.1	0.021	97.9%

2c	3 ML-FcC6SH	0.033×10^{-1}	190	110	0.36	0.044	86.7%
2a	5 ML-FcC6SH	0.093×10^{-2}	413	205	0.19	0.031	84.1%
2b	7 ML-FcC6SH	0.079×10^{-3}	890	446	0.035	0.021	60.5%
2c	3 ML-AlkylSH	0.028×10^{-2}	190	161	0.045	0.044	44.3%
3a	5 ML-AlkylSH	0.035×10^{-3}	413	387	0.014	0.031	27.3%
3b	7 ML-AlkylSH	0.078×10^{-4}	890	836	0.0065	0.021	22.1%
3c							

Family of Universal Curves

Table 1 tabulates the values of k_r, k_{ht}, OA_o (number of native oleic acid per QD), N_{max}, $N_{max}k_{ht}$, and the maximum HTQY (eqs 3a and 3b) for the nine systems depicted in Figure 4. N_{max} is the maximum number of hole accepting ligands that were experimentally measured in the respective system, and it corresponds to approximately the maximum number of ligands that could be exchanged by mixing at room temperature. As shown in Table 1, N_{max} depends on the size of the QD and the length of the alkyl chain of the acceptor.

$$\mathrm{HTQY} = \frac{Nk_{ht}}{k_r + k_{nr} + Nk_{ht}} = 1 - \frac{\mathrm{PLQY}(N)}{\mathrm{PLQY}(N=0)} \quad (3a)$$

$$\mathrm{HTQY}_{max} = \frac{N_{max}k_{ht}}{k_r + k_{nr} + N_{max}k_{ht}} = 1 - \frac{\mathrm{PLQY}(N_{max})}{\mathrm{PLQY}(N=0)} \quad (3b)$$

HTQY_{max} represents the maximum hole extraction yield achieved at the highest coverage, N_{max}. The nanocrystal systems with FcC3SH achieve HTQY_{max} of 97.9% to 99% at maximum coverage. k_{ht}, the hole transfer rate constant per acceptor, on the other hand, varies from 63 μs^{-1} for hole transfer from the 3 ML QD to the FcC3SH molecule to 7.8 ms^{-1} for hole transfer from the 7 ML QD to AlkylSH.

The ratio, r, relating the total hole transfer rate Nk_{ht} to the sum of the native pathways for recombination (eq 4) determines the curvature of each data set in Figure 4. This can be understood by examining the two limits of $r \ll 1$ and $r \gg 1$. The curvature depends on the range of N being examined, but since we are interested in understanding the curvature over the entire region of N ligands that the QD can accommodate, the approximation for r is done at $N = N_{max}$.

$$r = \frac{Nk_{ht}}{k_r + k_{nr}} \quad (4)$$

$$\mathrm{PLQY}\left(\frac{Nk_{ht}}{k_r + k_{nr}} \approx 0\right) = \mathrm{PLQY}_o - \mathrm{PLQY}_o\frac{k_{ht}}{k_r + k_{nr}}N \quad (5)$$

In the limit of $r \ll 1$ or $r \approx 0$, $k_r + k_{nr}$ is the dominant pathway for the recombination of photoseparated charges, even when the maximum number of acceptors, N_{max}, is bound. This limit can be approximated by a Taylor expansion of r about 0, which when applied to eq 2 produces a *linear relationship between PLQY and N* (eq 5) up to N_{max}. $PLQY_o$ is the PLQY of the QD when no charge acceptor ligands are bound.

System **3c**, which is the most inefficient hole transfer system, is the closest experimental example describing this limit, in which $N_{max}k_{ht}$ is slower than k_r; the plot of its PLQY as a function of coverage in Figure 4 is linear. Even at over 800 acceptors bound, the total hole transfer rate is still significantly slower than the k_r of the QD. This is the system with the thickest CdS shell in our study and with the low driving force thiol acceptor. To elaborate further, for many of the nine systems, this linear regime exists when examining N up to the value that validates the r approximation. For example, system **3b** would be linear up to $N = 40$, approximately one tenth of its maximal value.

In the other limit of $r \gg 1$, Nk_{ht} is larger than k_r. The inverse relationship in eq 2 is very steep such that small N has large effects on the PLQY. System **1a** demonstrates this limit at N_{max}: the $N_{max}k_{ht}$ in this system is over 2 orders of magnitude greater than $k_r + k_{nr}$, and the curvature shown in Figure 4 is representative of a highly inverse relationship. In the extreme examples of this limit, a single ligand charge acceptor can quench a significant portion of the QD fluorescence ($k_{ht} \sim k_r$) or even completely quench the fluorescence ($k_{ht} \gg k_r$). In our experiments, the k_{ht} of system **1a** is directly competitive with k_r. As shown in the logarithmic depiction of these relationships, one FcC3SH per QD in system **1a** is predicted to quench the PLQY from 79% to 37%. In other words, *a single acceptor* achieves a HTQY of 53%.

By modulating electronic coupling we were able to experimentally and systematically characterize eq 4 from one limit of r to the other. The other systems in this study represent the conditions that lie in between these two limits, where k_r and $N_{max}k_{ht}$ are more comparable and the equation cannot be reduced to the simpler forms.

By demonstrating that the linear and nonlinear relationships between PL intensity and coverage can both be achieved depending on r, we resolve the root of the conflicting results on this topic in the literature, which has depicted both these trends. As shown clearly and discussed previously, the ratio r determines the degree of linearity in the PLQY–N relationship. As r tends to 0, the relationship becomes linear. The myriad of linear and nonlinear observations in the literature(29, 31, 32) is a consequence of the variable systems and their

respective variant parameters, k_r, k_{ht}, and *N*. *N* is especially important in these measurements; given its variability, even if the approximation in eq 5 is invalid at $N = N_{max}$, smaller values of *N* may be valid for eq 5, and therefore, measurements up to that *N* will produce experimental data that describes a linear relationship. In systems with very effective k_{ht} such as systems **1a** and **1b**, there exist no values of *N* that give a linear relationship. The nine relationships we have shown here demonstrate that rather than being strictly linear or nonlinear, the PL coverage relationship is a function that has continuity from one extreme to the other.

Thiols versus Ferrocene

Hole transfer rates to the AlkylSH ligand are about 10% as fast as the hole transfer rates to the ferrocene ligands with thiolate binding groups. We thereby have excluded charge trapping to the thiolate binding group from being a convoluting or competitive pathway for hole transfer in the ferrocene donor–acceptor systems. However, assuming the total charge transfer to be a sum of both pathways, this reduces the hole transfer rates to ferrocene acceptors by up to 10%. In this experiment, the larger band gap CdS shell has a high enough energy barrier such that the hole transfer to intrinsic nonradiative pathways and low-driving force traps like thiols is ineffective, while at the same time being weak enough so that tunneling to a high driving force acceptor such as ferrocene is effective. This thereby demonstrates that one can use QD heterostructure design to strike a balance between mitigating undesirable traps while still being able to extract charge efficiently to well-defined desirable traps.

k_{ht} versus HTQY

In Table 1, we pay special attention to k_{ht} and $HTQY_{max}$, as they together comprehensively describe the effectiveness of nanocrystal charge transfer. More specifically, k_{ht} depicts the individual charge transfer efficiency of each ligand while HTQY (eq 3) is the efficiency of the entire QD system to extract the photogenerated hole from the core to the surface. Therefore, HTQY includes contributing factors from the competing pathways of k_r and the number of acceptors bound, *N*. While k_{ht} is an intrinsic parameter that can be compared to the theory of charge transfer, HTQY is an extensive empirical value with implications for applications in energy conversion, with $HTQY_{max}$ representing the charge transfer efficiency limit of a QD-molecular system at maximum acceptors bound. Both are essential for understanding nanocrystal charge transfer.

a**k_{ht} for Reliable Comparisons Between Systems to Examine Electronic Coupling**

The k_{ht} values obtained allow us to accurately investigate the effects of coupling under calibrated conditions. The distance dependence of the charge transfer rate constant is described by eq 6, where *d* is the distance of the energy barrier and β is an empirical damping coefficient that describes the extent of coupling through

the barrier material. By varying the shell thickness and obtaining the resulting k_{ht}, we can determine β for hole transfer through CdS. Figure 5 shows the plot of the logarithm of k_{ht} as a function of the thickness of CdS for the FcC3SH, FcC6SH, and AlkylSH systems, yielding β for hole transfer of (0.22 ± 0.032), (0.26 ± 0.022), and (0.25 ± 0.021) $Å^{-1}$, respectively. The values are within error of each other, yielding an average β of (0.24 ± 0.025) $Å^{-1}$, which is similar to electron transfer through conjugated carbon chains with reported β values of ~0.2 $Å^{-1}$. A higher β indicates weaker coupling, or higher tunneling barrier, since the rate drops off at shorter distances. Previous work on charge transfer on semiconductor nanocrystal heterostructures has measured β of 0.91 $Å^{-1}$ for hole transfer through ZnS in a CdSe/ZnS system.(41) This measurement differs from our system in that its hole transfer is the recombination step after electron transfer and therefore is independent of the number of acceptors. As the valence band of ZnS lies lower in energy than that of CdS, we expect the lower CdS barrier to result in higher coupling between the donor and acceptor, and hence a lower β, which agrees with the experimental results. In addition, the difference in the hole effective mass between CdS and ZnS also contributes to the lower β measured.

$$k_{ht}(d) = k_o e^{-\beta d} \quad (6)$$

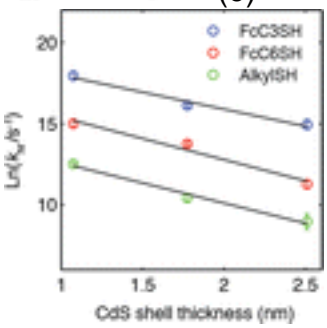

Figure 5. Hole transfer through CdS yields β of (0.24 $^{-1}$ ± 0.03) $Å^{-1}$.

We additionally calculated β for hole transfer through the saturated carbon bonds of the ferrocene ligand by comparing the k_{ht} for FcC3SH versus FcC6SH. This yields β of ~(0.85 ± 0.1) $Å^{-1}$, which falls within what has been experimentally measured for saturated carbon chains in literature.(7) These two β measurements together increase our confidence that the donor–acceptor distance is well-defined in our charge transfer system.

Furthermore, we can use these β values to predict the k_{ht} for hole transfer from bare CdSe QD to acceptors that are separated from the surface by a single bond. For a CdSe core with a diameter of 3.9 nm containing approximately 30 acceptor ligands, we predict a single hole transfer time constant of about 200 ps and a total hole transfer rate below 10 ps. This value is comparable to ref 15 for hole transfer from CdSe to various Ru-polypyridine complexes with similar driving

force and similar donor–acceptor distance as our system. However, it is faster than the 2.5 ns rate measured for hole transfer from CdSe to phenothiazine physisorbed to the surface in a 1:1 donor–acceptor mixture,(16) which agrees with findings that electronic coupling via van der Waals forces is much weaker than those achievable through covalent interactions.(42)

b**HTQY and the Possible Advantages of Multiple Acceptors**

The QD itself is stable upon electronic excitation because one quantum of electronic excitation is distributed over thousands or even tens of thousands of atoms. When hole transfer takes place for a system with one molecular acceptor, the charge is now confined within just the few atoms of the molecular acceptor. The molecular acceptor is therefore more likely to degrade by charge transfer dynamics before the QD does. This is the root cause of the enhanced photochemical stability of QDs over molecular chromophores. Yet by balancing rates and the number of ligands, we show that it is possible to assemble one QD with hundreds of molecular acceptors so that the degradation of one acceptor will not render the entire system inactive for further hole transfer. The ability to distribute the probability of hole transfer into many acceptors on the surface may be a strategic advantage of nanocrystal systems. Additionally, by using a molecule with a well-defined redox potential, we achieve specificity in the driving force for hole transfer. The high number of hole transfer pathways in these systems therefore provides a means by which charge transfer can occur both effectively, persistently, and specifically.

In molecular systems commonly made of a single donor and a single acceptor, the charge transfer rate k_{ct} must outcompete the native recombination pathways to be effective. For example, electron transfer from $[Ru(bpy)_3]^{2+}$ to methyl viologen is effective because the electron transfer time constant of tens of nanoseconds is much faster than the microsecond triplet lifetime of the sensitizer. Table 1 shows that, in the QD-molecular systems explored here, only in system **1a** does the k_{ht} (63 μs^{-1}) surpass k_r (44 μs^{-1}). In this system, with contribution from approximately 91 acceptor ligands, the $N_{max}k_{ht}$ of the system reaches 5.8 ns^{-1}, or a total time constant of 170 ps, which is more than 2 orders of magnitude faster than the 23 ns radiative lifetime of the QD with 3 ML shell. The $HTQY_{max}$ for this system is approximately unity.

On the other hand, for six out of the nine donor–acceptor systems studied here, the k_{ht} is 1 to over 4 orders of magnitude slower than k_r. This highlights one of the important advantages of QD charge transfer as a single donor-multiple acceptor system. The addition of more acceptors can compensate for the intrinsically low k_{ht} as compared to k_r, as is the case for the systems **2a**, **2b**, and **2c**. Although a thicker shell lowers k_{ht}, the number of acceptors that can be accommodated on this larger QD grows as the square of the radius. Therefore, $N_{max}k_{ht}$ does not drop off at the same magnitude as k_{ht} over the same coupling distance, as shown

in Figure 6. Additionally, k_r, the competitive pathway for charge recombination, is a tunable parameter that also affects the efficiency of hole extraction in these systems, as it approximately doubles from the 7 ML QD to the 3 ML QD.

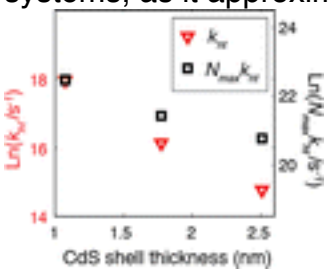

Figure 6. Comparison of k_{ht} versus Nk_{ht} as a function of the three shell thicknesses for hole transfer to FcC3SH. At larger sizes, N increases as the square of the radius, thereby lessening the magnitude of the decrease in Nk_{ht}.

To illustrate this point further, we see that system **2a** has a higher k_{ht} but a lower HTQY$_{max}$ than system **1c**. System **2a** is more effective as a single donor-*single* acceptor system, with a faster k_{ht}, but system **1c** is more effective as a single donor-*multiple* acceptor system. System **1c** is able to accommodate over 3 times as many ligands as system **2a**, and thus, it is able to achieve a higher total charge transfer rate $N_{max}k_{ht}$ and therefore a higher HTQY$_{max}$. Additionally, its k_r is slower than that of system **2a** making it easier for hole transfer to outcompete native recombination pathways. Similarly, systems **3a** and **2c** depict the same trend.

AlkylSH is able to achieve the highest maximum coverage (Table 1) for the same QD size because the pyrrole group comfortably occupies the spatial volume at a distance that is 11 carbon molecules from the QD surface. On the other hand, FcC6SH with its six carbon linker and FcC3SH with its three carbon linker are more kinetically inhibited to bind at higher coverages due to the steric effects of the cyclopentadiene rings at these close distances from the QD surface. Additionally, the maximum achieved coverage is greater for FcC6SH than FcC3SH, as expected. Similar to the effects seen in modulating CdS shell thickness, a higher N_{max} afforded by the longer chain length linearly improves the total hole transfer rate $N_{max}k_{ht}$ as a result of improved packing; k_{ht} on the other hand drops exponentially over this distance due to the weaker electronic coupling at this longer chain length. Notably, the larger β (0.85 Å^{-1}) of the alkyl chain than that of the CdS shell (0.24 Å^{-1}) indicates that N_{max} achieved by modulating the chain length plays a smaller role in counteracting the effect of electronic coupling. The effect on a plot of $N_{max}k_{ht}$ in Figure 6 versus shell thickness will be less pronounced for the ligand shell than the inorganic CdS shell.

Both HTQY and k_{ht} are important in the characterization of nanocrystal charge

transfer. While k_{ht} allows one to accurately compare systems as a function of variation in the parameters of charge transfer theory, HTQY reflects the efficiency of the entire system to extract the hole to the surface. $HTQY_{max}$ represents the best charge transfer efficiency one can obtain from such a QD system. Therefore, the often-overlooked factors of k_r and N can have a significant effect on charge transfer efficiency.

•

Conclusion

We examined hole transfer in nine donor–acceptor systems covering a broad range of hole transfer rates modulated by electronic coupling. The hole donor is the CdSe of the CdSe-core CdS-shell nanocrystal with either a 3, 5, or 7 ML CdS shell, and the acceptors are the high driving force hole accepting ferrocene moiety and the low driving force thiol. Two different alkyl chain lengths for the ferrocene ligand were used. We measured the PLQYs for these systems over a range of acceptor coverages. From this data, we extracted the hole transfer rate constant per acceptor, k_{ht}, and the maximum hole transfer quantum yield, $HTQY_{max}$. The empirical damping coefficient β for the CdS shell barrier is determined to be (0.24 ± 0.025) $Å^{-1}$. The β for the alkyl chain is (0.85 ± 0.1) $Å^{-1}$, in agreement with what is predicted for tunneling through unsaturated carbon bonds, which demonstrates that these donor–acceptor systems have well-defined distances. k_{ht} is a fundamental constant that describes the nature of the single-donor single-acceptor system obeying the parameters given in Marcus theory. HTQY on the other hand incorporates the empirical parameters of the nanocrystal systems: radiative rate constant and the total number of bound hole acceptors. Both parameters are essential for characterizing charge transfer. The nine donor–acceptor systems also demonstrate that the PL coverage relationship can be varied from nonlinear to linear by modulating the ratio of the total hole transfer rate to the sum of the native recombination rates in the QD. By understanding the PL coverage relationship, we can more accurately utilize PL as an indirect probe for studying ligand-binding equilibrium as is often done in literature.

In these studies, we show that high PLQY samples (>79%) that are passivated by CdS shells can still reach charge transfer efficiencies up to 99% due to the large surface area of the particles that allows for binding of many acceptor ligands, thus increasing k_{ht} by a factor of up to over 800 compared to a single-donor single-acceptor system. The single charge transfer lifetime and the total charge transfer lifetime for the fastest system in our studies are 16 ns and 170 ps, respectively. Charge transfer studies in the literature have been mostly done on low PLQY, trap-heavy particles.(8) In these trap-heavy particles, charge transfer must compete with the native highly fluctuating nonradiative pathways. In contrast, we demonstrate through these studies that one can use the design of

QD heterostructures and acceptor ligands to mitigate undesirable and ill-defined traps, while still being able to extract the charge efficiently to desirable traps with specificity in energy level, physical and electronic interaction, and quantity. In doing so, we can achieve high photostability and high charge transfer efficiency concurrently.

•

Experimental Methods

Chemicals

6-(Ferrocenyl)hexanethiol (FcC3SH), ferrocene (Fc, 98%, sublimed), 11-(1*H*-pyrrol-1-yl)undecane-1-thiol (PyrrSH), 3-bromopropionyl chloride, sodium cyanoborohydride ($NaBH_3CN$, 95%), tetra-*n*-butylammonium fluoride (TBAF), boron trifluoride diethyl etherate (BF_3OEt_2), aluminum chloride ($AlCl_3$), oleic acid (OA, 90%), 1-octadecene (ODE, 90%), oleylamine (OLAM, 70%), chloroform-*d*, and selenium (Se, 99.99%) were purchased from Sigma-Aldrich. Other chemicals used are hexamethyldisilathiane ($S(SiMe_3)_2$, Fluka), magnesium sulfate ($MgSO_4$, EMD), ammonium hydroxide (14.8 M, EMD), sodium chloride (NaCl, EMD), hydrochloric acid (HCl, 12 M, Fischer Scientific), silica gel (FLASH, 40–63 μm), cadmium oxide (CdO, 99.99%, Alfa Aesar), tri-n-octylphosphine oxide (TOPO, 99%, Strem), tri-n-octylphosphine (TOP, 99%, Strem), octadecylphosphonic acid (ODPA, 99%, PCI Synthesis), sulfur (S, 99.9995% Alfa Aesar), Bio-Beads S-X3 Beads (Biorad), tetrabutylammonium hexafluorophosphate (TBAH-PF6, 99.0+%, Fluka), Cd^{2+} Standard for ICP (Fluka), nitric acid (65%, TraceSELECT Ultra, Fluka), and the anhydrous solvents chloroform, acetone, methanol, toluene, tetrahydrofuran, dichloromethane, and acetonitrile.

CdSe-Core CdS-Shell Synthesis

CdSe-core CdS-shell nanocrystals were synthesized by modifying a previously published procedure.(43) The cadmium precursor for CdS growth was made by mixing CdO with 10 equiv of OA and the needed quantity of ODE to reach 0.2 M concentration of cadmium oleate, heating at 250 °C under argon until the solution turned clear, and degassing at 100 °C for 30 min. Appropriate amounts of octanethiol and ODE were mixed to prepare the 0.2 M octanethiol solution, which served as the sulfur precursor. Depending on the desired thickness of CdS, the moles of precursors required were calculated, and the correct volume of the precursor solutions was subsequently injected together. A 50 mL three-neck round-bottom flask equipped with a reflux condenser and a thermocouple was charged with CdSe QDs (200 nmol measured by the first exciton(44)), 3 mL of OLAM, and 3 mL of ODE. The mixture was heated to 310 °C to react, and the injections of the Cd and S precursors began at 250 °C at a rate of 3 mL/hour. Once the injections were finished, the flask was cooled, and the CdSe-core CdS-shell nanocrystals were isolated from the ligand mixture by precipitating the particles in acetone, redispersing them in hexane, and repeating this procedure two more times.

Synthesis of 3-(Ferrocenyl)propylthiol (FcC3SH)

FcC3SH was synthesized via a combination of previous literature preparations.(45, 46) See Supporting Information for details.

Ligand Exchange with CdSe-Core CdS-Shell Particles

Hole acceptor ligands FcC6SH, FcC3SH, and AlkylSH were exchanged onto the particles by adding the ligands to the nanocrystal solutions in chloroform at room temperature. Thiolates readily displace native oleic acid ligands on the nanocrystal surface. The extent of the exchange was controlled by the concentration of added ligands, as the exchange reaches equilibrium within minutes. After ligand exchange, the free ligands were removed in two ways. For FcC3SH and FcC6SH, a chloroform–acetonitrile precipitation was used to remove the free ligands through the disposure of the supernatant. For Alkyl-SH, the conventional precipitation method irreversibly aggregated the particles so size-selective chromatography using porous polystyrene beads separated the free ligands from the nanocrystals.(47) Both methods are effective, as shown by the lack of free ligands in the NMR of the cleaned products. Additionally, we show that our methods of cleaning have no effect on the PLQY of the QDs (Supporting Information Figure S5).

Optical Spectroscopy

All optical measurements were performed on tens to hundreds of nanomolar concentrations of particles dispersed in chloroform. Absorption spectra were collected on a Shimadzu 3600 spectrophotometer with 1 nm increments and chloroform background subtraction. Photoluminescence emission spectra were collected on a Horiba Jobin Yvon TRIAX 320 Fluorolog. Fluorescence lifetime was collected on a Picoquant Fluotime 300 with PMA 175 detector and an LDH-P-C-405 diode laser (excitation wavelength of 407.1 nm). Quantum yields are determined by measuring the fluorescence intensity of the nanocrystals against Rhodamine 6G.

Quantitative NMR

Quantitative NMR spectra of micromolar concentrations of CdSe/CdS core–shell particles were measured on a Bruker 400 MHz instrument. Digital ERETIC (Bruker Topspin) was used to determine the concentration of ligands, which is an instrumental implementation of the PULCON (pulse length based concentration determination)(37) method. In this method, a known concentration of a standard (10 mM of ferrocene in $CDCl_3$ in the current study) was measured on the instrument after tuning the probe and measuring the exact 90° radio frequency pulse. The ferrocene peak was integrated, and the known concentration was entered and stored into the software for that peak. When measuring the concentration of the ligand protons in the nanocrystal sample, the same receiver gain value was used, the probe was tuned, and the 90° pulse was determined and used. Digital ERETIC was implemented in the software by converting the absolute integration measured to concentration; at the same time, a synthetic peak was generated in the spectrum as a reference to concentration. Note that one can determine quantitative concentration without the software functionality as

well, by comparing the absolute integration values divided by the number of scans of the known standard with that of the unknown concentration sample; this method is highlighted in ref 37.

ICP Atomic Emission Spectroscopy

Nanocrystal concentration was determined by measuring the Cd^{2+} concentration using an Optima 7000 DV ICP-AES (Perkins Elmer) and calculating the number of Cd atoms per nanocrystal for the given size as determined via transmission electron microscopy (TEM). Cadmium ICP standards serially diluted to cover a range of concentrations were measured to generate a calibration curve. Nanocrystal samples are prepared by evacuating a 200 μL aliquot of the stock solution, and then adding 500 μL of nitric acid to digest the particles for a few hours. The solutions were then diluted in Millipore water in the same series of dilutions as the Cd^{2+} ICP standards, and measured.

Supporting Information

Experimental descriptions and data on cyclic voltammetry, transmission electron microscopy (TEM), synthesis of molecular ligands, further characterization of nanocrystal surface, and controls. This material is available free of charge via the Internet at http://pubs.acs.org.

The authors declare no competing financial interest.

•

Acknowledgment

This work is supported by the Physical Chemistry of Inorganic Nanostructures Program, KC3103, Office of Basic Energy Sciences of the United States Department of Energy under Contract DE-AC02-05CH11232. T.X.D and J.H.O. acknowledge the National Science Foundation Graduate Research Fellowship under Grant DGE 1106400, and their research peers Brandon Beberwyck and Noah Bronstein for helpful discussions.

• Reference QuickView

•

References

This article references 47 other publications.

1. Pinaud, F.; Clarke, S.; Sittner, A.; Dahan, M. *Nat. Methods* **2010**, 7, 275– 285[CrossRef], [PubMed], [CAS]
2. Coe-Sullivan, S.; Steckel, J. S.; Kim, L.; Bawendi, M. G.; Bulović, V. *Proc. SPIE* **2005**, 5739, 108– 115[CrossRef], [CAS]
3. Chen, X.; Shen, S.; Guo, L.; Mao, S. S. *Chem. Rev.* **2010**, 110, 6503– 6570[ACS Full Text], [PubMed], [CAS]
4. Kamat, P. V. *J. Phys. Chem. C* **2008**, 112, 18737– 18753[ACS Full Text], [CAS]
5. Marcus, R. A.; Sutin, N. *Biochim. Biophys. Acta* **1985**, 811, 265– 322[CrossRef], [CAS]
6. Barbara, P. F.; Meyer, T. J.; Ratner, M. A. *J. Phys. Chem.* **1996**, 100,

13148– 13168[ACS Full Text], [CAS]
7. Adams, D. M.; Brus, L.; Chidsey, C. E. D.; Creager, S.; Creutz, C.; Kagan, C. R.; Kamat, P. V.; Lieberman, M.; Lindsay, S.; Marcus, R. A.; Metzger, R. M.; Michel-Beyerle, M. E.; Miller, J. R.; Newton, M. D.; Rolison, D. R.; Sankey, O.; Schanze, K. S.; Yardley, J.; Zhu, X. *J. Phys. Chem. B* **2003**, 107, 6668– 6697[ACS Full Text], [CAS]
8. Knowles, K. E.; Peterson, M. D.; McPhail, M. R.; Weiss, E. A. *J. Phys. Chem. C* **2013**, 117, 10229– 10243[ACS Full Text], [CAS]
9. Zhu, H.; Yang, Y.; Hyeon-Deuk, K.; Califano, M.; Song, N.; Wang, Y.; Zhang, W.; Prezhdo, O. V.; Lian, T. *Nano Lett.* **2014**, 14, 1263– 1269[ACS Full Text], [PubMed], [CAS]
10. Morris-Cohen, A. J.; Frederick, M. T.; Cass, L. C.; Weiss, E. A. *J. Am. Chem. Soc.* **2011**, 133, 10146– 10154ACS Full Text, [PubMed], [CAS]
11. Boulesbaa, A.; Huang, Z.; Wu, D.; Lian, T. *J. Phys. Chem. C* **2010**, 114, 962– 969[ACS Full Text], [CAS]
12. Boulesbaa, A.; Issac, A.; Stockwell, D.; Huang, Z.; Huang, J.; Guo, J.; Lian, T. *J. Am. Chem. Soc.* **2007**, 129, 15132– 15133ACS Full Text, [PubMed], [CAS]
13. Burda, C.; Green, T. C.; Link, S.; El-Sayed, M. A. *J. Phys. Chem. B* **1999**, 103, 1783– 1788[ACS Full Text], [CAS]
14. Sharma, S. N.; Pillai, Z. S.; Kamat, P. V. *J. Phys. Chem. B* **2003**, 107, 10088– 10093[ACS Full Text], [CAS]
15. Sykora, M.; Petruska, M. A.; Alstrum-Acevedo, J.; Bezel, I.; Meyer, T. J.; Klimov, V. I. *J. Am. Chem. Soc.* **2006**, 128, 9984– 9985ACS Full Text, [PubMed], [CAS]
16. Huang, J.; Huang, Z.; Jin, S.; Lian, T. *J. Phys. Chem. C* **2008**, 112, 19734– 19738[ACS Full Text], [CAS]
17. Song, N.; Zhu, H.; Jin, S.; Lian, T. *ACS Nano* **2011**, 5, 8750– 8759[ACS Full Text], [PubMed], [CAS]
18. Tseng, H.-W.; Wilker, M. B.; Damrauer, N. H.; Dukovic, G. *J. Am. Chem. Soc.* **2013**, 135, 3383– 3386ACS Full Text, [PubMed], [CAS]
19. Tarafder, K.; Surendranath, Y.; Olshansky, J. H.; Alivisatos, A. P.; Wang, L.-W. *J. Am. Chem. Soc.* **2014**, 136, 5121– 5131ACS Full Text, [PubMed], [CAS]
20. Wu, K.; Chen, Z.; Lv, H.; Zhu, H.; Hill, C. L.; Lian, T. *J. Am. Chem. Soc.* **2014**, 136, 7708– 7716ACS Full Text, [PubMed], [CAS]
21. Kamat, P. V.; Christians, J. A.; Radich, J. G. *Langmuir* **2014**, 30, 5716– 5725[ACS Full Text], [PubMed], [CAS]
22. Klimov, V.; McBranch, D.; Leatherdale, C.; Bawendi, M. *Phys. Rev. B* **1999**, 60, 13740– 13749[CrossRef], [CAS]
23. Fisher, B. R.; Eisler, H.-J.; Stott, N. E.; Bawendi, M. G. *J. Phys. Chem. B* **2004**, 108, 143– 148[ACS Full Text], [CAS]
24. Aldana, J.; Lavelle, N.; Wang, Y. J.; Peng, X. G. *J. Am. Chem. Soc.* **2005**, 127, 2496– 2504ACS Full Text, [PubMed], [CAS]

25. Schrier, J.; Wang, L.-W. *J. Phys. Chem. B* **2006**, 110, 11982–11985[ACS Full Text], [PubMed], [CAS]
26. Sadhu, S.; Tachiya, M.; Patra, A. *J. Phys. Chem. C* **2009**, 113, 19488–19492[ACS Full Text], [CAS]
27. Koposov, A. Y.; Szymanski, P.; Cardolaccia, T.; Meyer, T. J.; Klimov, V. I.; Sykora, M. *Adv. Funct. Mater.* **2011**, 21, 3159– 3168[CrossRef], [CAS]
28. Li, X.; Nichols, V. M.; Zhou, D.; Lim, C.; Pau, G. S. H.; Bardeen, C. J.; Tang, M. L. *Nano Lett.* **2014**, 14, 3382– 3387[ACS Full Text], [PubMed], [CAS]
29. Munro, A. M.; Jen-La Plante, I.; Ng, M. S.; Ginger, D. S. *J. Phys. Chem. C* **2007**, 111, 6220– 6227[ACS Full Text], [CAS]
30. Ji, X.; Copenhaver, D.; Sichmeller, C.; Peng, X. *J. Am. Chem. Soc.* **2008**, 130, 5726– 5735ACS Full Text, [PubMed], [CAS]
31. Bullen, C.; Mulvaney, P. *Langmuir* **2006**, 22, 3007– 3013[ACS Full Text], [PubMed], [CAS]
32. Anderson, N. C.; Hendricks, M. P.; Choi, J. J.; Owen, J. S. *J. Am. Chem. Soc.* **2013**, 135, 18536– 18548ACS Full Text, [PubMed], [CAS]
33. Munro, A. M.; Ginger, D. S. *Nano Lett.* **2008**, 8, 2585– 2590[ACS Full Text], [PubMed], [CAS]
34. She, C.; Demortiere, A.; Shevchenko, E. V.; Pelton, M. *J. Phys. Chem. Lett.* **2011**, 2, 1469– 1475[ACS Full Text], [CAS]
35. Dorokhin, D.; Tomczak, N.; Velders, A. H.; Reinhoudt, D. N.; Vancso, G. J. *J. Phys. Chem. C* **2009**, 113, 18676– 18680[ACS Full Text], [CAS]
36. Wuister, S. F.; de Mello Donegá, C.; Meijerink, A. *J. Phys. Chem. B* **2004**, 108, 17393– 17397[ACS Full Text], [CAS]
37. Wider, G.; Dreier, L. *J. Am. Chem. Soc.* **2006**, 128, 2571– 2576ACS Full Text, [PubMed], [CAS]
38. Puzder, A.; Williamson, A. J.; Zaitseva, N.; Galli, G.; Manna, L.; Alivisatos, A. P. *Nano Lett.* **2004**, 4, 2361– 2365[ACS Full Text], [CAS]
39. Gomes, R.; Hassinen, A.; Szczygiel, A.; Zhao, Q.; Vantomme, A.; Martins, J. C.; Hens, Z. *J. Phys. Chem. Lett.* **2011**, 2, 145– 152[ACS Full Text], [CAS]
40. Garcia-Santamaria, F.; Brovelli, S.; Viswanatha, R.; Hollingsworth, J. A.; Htoon, H.; Crooker, S. A.; Klimov, V. I. *Nano Lett.* **2011**, 11, 687–693[ACS Full Text], [PubMed], [CAS]
41. Zhu, H.; Song, N.; Lian, T. *J. Am. Chem. Soc.* **2010**, 132, 15038–15045ACS Full Text, [PubMed], [CAS]
42. Chaban, V. V.; Prezhdo, V. V.; Prezhdo, O. V. *J. Phys. Chem. Lett.* **2013**, 4, 1– 6[ACS Full Text], [PubMed], [CAS]
43. Chen, O.; Zhao, J.; Chauhan, V. P.; Cui, J.; Wong, C.; Harris, D. K.; Wei, H.; Han, H.-S.; Fukumura, D.; Jain, R. K.; Bawendi, M. G. *Nat. Mater.* **2013**, 12, 445– 451[CrossRef], [PubMed], [CAS]
44. Yu, W. W.; Qu, L.; Guo, W.; Peng, X. *Chem. Mater.* **2003**, 15, 2854–

2860[ACS Full Text], [CAS]
45. Müller-Meskamp, L.; Karthäuser, S.; Waser, R.; Homberger, M.; Wang, Y.; Englert, U.; Simon, U. *Surf. Sci.* **2009**, 603, 716–722[CrossRef], [CAS]
46. Tindale, J. J.; Hartlen, K. D.; Alizadeh, A.; Workentin, M. S.; Ragogna, P. J. *Chem.—Eur. J.* **2010**, 16, 9068– 9075[CrossRef], [PubMed], [CAS]
47. Shen, Y.; Gee, M. Y.; Tan, R.; Pellechia, P. J.; Greytak, A. B. *Chem. Mater.* **2013**, 25, 2838– 2848[ACS Full Text], [CAS]